Available online at www.sciencedirect.com
SCIENCE DIRECT®
Journal of Nuclear Materials 324 (2004) 203–214
journal of nuclear materials
www.elsevier.com/locate/jnucmat

Cathodoluminescence imaging of oxidised zirconium alloys

H. Ken Yueh *, Brian Cox

Centre for Nuclear Engineering, University of Toronto, 184 College Street, Toronto, Ont., Canada M5S 3E4

Received 25 August 2003; accepted 7 October 2003

Abstract

Cathodoluminescence (CL) imaging techniques have been applied to the characterisation of the zirconium oxide films formed from binary Zr alloy matrices using a homemade CL imaging system attached to an Hitachi S-570 scanning electron microscope (SEM). Evidence from the CL images shows the involvement of the individual Zircaloy alloying elements in the luminescence process. β-annealed and slow-cooled samples which have strongly segregated alloying elements at their grain boundaries showed strong CL signals from these areas. Use of this heat treatment was necessary to compensate for the low resolution of the equipment. Strong CL signals were observed also from cracks in the oxides on some alloys and are believed to be caused by the redistribution of iron to the region adjacent to the crack, but below the original surface. Increasing redistribution of Fe with increasing oxidation temperature is seen in the CL images. The cyclic behaviour observed in the weight gain measurements is also observed in the CL intensity measurements. Experimental data from this investigation support the theory that this phenomenon is caused by the successive formation of cracks parallel and normal to the plane of the metal matrix.

1. Introduction

Zirconium alloys such as Zircaloy-2 and Zircaloy-4 are widely used in the cores of water cooled nuclear reactors. The solubility limits for the common alloying elements (Fe, Cr, Ni) are generally low; as low as 100 ppm by weight for Fe, Cr and Ni at reactor operating temperatures. Existing techniques for non-destructive chemical analysis do not have the sensitivity required for their detection in the metal matrix, since most of these elements are precipitated. The alloying element distributions in the final oxide have important impacts on the oxidation rate of the alloy [1]. It is, therefore, necessary to use an alternative inspection technique that is capable of detecting the alloying elements at the low concentrations present in the matrix between the intermetallic precipitate particles.

In a preliminary study, luminescence techniques were shown to have the required sensitivity for this purpose [2]. However, there is no unified quantitative theory for the origin of these signals. In addition, there is no published literature data on the luminescence properties of zirconium oxide films formed from a metallic substrate. There are numerous publications on stabilised bulk zirconia [3–10] and these reports suggest that oxygen vacancies and/or impurities are involved in the luminescence process. One of the earliest hypotheses attributed the luminescence in the zirconium oxide system to titanium impurity ions. Later theories linked the involvement of oxygen vacancies to the luminescence process. The three major competing hypotheses for the explanation of the luminescence process in the zirconium oxide system involving oxygen vacancies have been discussed already [2] and it was concluded that specific impurities in a complex with vacancies are the origin of the luminescence. The specific details of the impurity-vacancy complex are discussed in Section 3.3. If the luminescence signals could be linked to some of the alloying additions in commercial zirconium alloys, this method could be ideally suited for the imaging of

* Corresponding author. Tel.: +1-803 647 3836; fax: +1-803 695 3973.
E-mail address: yuehk@westinghouse.com (H.K. Yueh).

0022-3115/$ - see front matter © 2003 Elsevier B.V. All rights reserved.
doi:10.1016/j.jnucmat.2003.10.003

the distributions of the alloying elements in the oxides on zirconium alloys. The preliminary study showed that this technique was worthy of further investigation, and this paper presents the results obtained from the cathodoluminescence imaging of a series of oxidised binary zirconium alloys doped with the various alloying elements present in the Zircaloys, using the same home made imaging system with relatively low resolution described previously [2].

2. Experimental procedure

Small buttons (~5 g) of binary alloys of zirconium and various elements of interest were made using a non-consumable tungsten arc furnace at concentrations of 0.1% and 0.5% by weight. The base zirconium metal was in the form of thin sheets which was used as the starting material. Each alloy was made by wrapping the zirconium foil around the dopant and melting it in the arc furnace. Each sample was flipped and remelted four times before removal from the arc furnace for further processing. A list of alloys is shown in Table 1 and the chemical purity of the materials used is listed in Table 2. The resultant melts took the form of flattened spherical buttons. To facilitate cutting, the buttons were flattened further in a hydraulic press and cut with a diamond-impregnated disk saw into smaller pieces. The smaller pieces were then flattened again into thin (1–2 mm thick) sheets before being vacuum sealed inside a fused silica tube for annealing. Samples were annealed for 24 h at 1273 K and allowed to cool in the furnace. All of the binary samples were oxidised in air at 723 K and later at 873 K after the oxide formed at 723 K was removed. These samples were studied for their CL surface features as well as CL intensities as a function of oxide thickness.

Table 2
Purity and form of the materials used in making metallic binary alloys

Element	Purity (%)	Form
Zr	99.94	Thin sheet
Cr	99	Pieces
Ni	99.99	Wire
Fe	99.9	Wire
Sn	99.9985	Wire

The CL attachment was made to fit a Hitachi S-570 model scanning electron microscope (SEM). A schematic diagram of the apparatus set up for CL imaging and a description of its construction was given in Ref. [2]. The light collection efficiency is in the order of 20% of the total emission. Due to the low light collection efficiency and low emission signal strength of some of the specimens, the effective spatial resolution was limited to less than 400×. Therefore, it was necessary to β-anneal specimens to obtain large clearly recognisable structural features.

3. Results and discussion

3.1. Examination before oxidation

The binary alloy samples were examined using the SEM and X-ray techniques to identify the chemical make up of the precipitates. The precipitates of the ZrCr system were small (less than half of a micrometer in diameter) compared to the precipitates of the other

Table 1
List of alloys

Sample designation	Alloy	Comments
A	Zr–0.1%Cr	Metallic binary alloys using 99.94% Zr base for oxide structure examination
B	Zr–0.5%Cr	
C[a]	Zr–0.1%Ni	
D	Zr–0.5%Ni	
E	Zr–0.1%Fe	
F	Zr–0.5%Fe	
G	99.94% zirconium sheet	Pure Zr melted without doping
IA	Zr–0.1%Cr	From the same melts as listed above (A, C, E and G) prepared for signal strength measurements
IC	Zr–0.1%Ni	
IE	Zr–0.1%Fe	
IG	Pure Zr melted, no doping	
AR	99.94% sheet, as received	ARA was annealed in vacuum at 1273 K for 24 h and furnace cooled
ARA	β-annealed AR	

[a] C was contaminated with Cu during the melting process.

alloying elements. In some cases, Fe impurity was found in the precipitates. Most of the precipitates were distributed along the Widmanstatten platelet (grain) boundaries with only a few inside the grains. Precipitates in the ZrFe and ZrNi systems were much larger than the precipitates in the ZrCr system. For the case of ZrFe alloys, sizes ranged from a fraction of a micrometer to 5 μm were common and were located mostly at grain boundaries. ZrNi precipitates were the largest of the 3 types studied, they ranged from a fraction of a micrometer to more than 10 μm in size and were exclusively distributed along the grain boundaries. An undoped sample of as-received zirconium sheet was also melted in the same arc furnace using the same melting routine. The original material contained up to 0.05% Fe which showed up as small Zr_3Fe precipitates, generally less than 1 μm in size. A small amount of Cr was also present in the as-received material; micro-X-ray examination of the precipitates confirmed that the amount of Cr in them was very low.

3.2. Contrast mechanism

At the beginning of this investigation, the source of the CL contrast in the samples was a big puzzle. It was not possible to relate this contrast simply to the surface appearance of the sample. To improve the information from the surface examination, two techniques were used to further the understanding of the contrast mechanism. One of the techniques involved the removal of the metal substrate on a small area of the oxide so that both sides of the oxide might be examined. The other method was to examine the edge profile, or cross section, of the oxide. Fig. 1 shows the images of a sample with an area of its metal substrate removed. One clearly sees from the CL image of this sample that strong CL signals are emitted in the vicinity of the prior metal grain boundaries which were broadened by the large amount of oxidised intermetallic originally present in them, and gave rise to the locally enhanced oxidation. In some cases, the signals originated not within the boundary (thick oxide) region, but were apparently on both sides of the boundary. From this it is not clear whether the stronger CL signals arise from the thicker oxide present in the boundary area or because of local chemical differences in the boundary region. This question is better answered by looking at the section of a sample, which is shown in Fig. 2. The composite image shown in part (c) of this figure best illustrates the point. There is a clear correlation between the features seen in the top view and the section. These correlated images clearly show that the high CL intensity areas near the grain boundary regions arise not just because of the thicker oxide at these locations. The combination of these experiments suggests that the contrast in images obtained from specimen surfaces arise because of a combination of the greater oxide thickness and high CL signals due to chemical segregation effects. Since the oxide is quite transparent to light in the 500 nm wavelength range, it is reasonable to assume that the light emissions from different depths in the oxide are additive and therefore will produce an enhanced signal when imaged from the surface. The optical transmission properties of the oxides of pure zirconium and a Zr–0.5%Cu–0.5%Mo alloy were measured at different oxide thicknesses [2]. Absorption coefficients of 0.15 and 0.35 per micrometer of oxide were calculated for these two materials, respectively. The lower absorption coefficient of the pure zirconium oxide is consistent with the observed CL intensity increase up to an oxide thickness of approximately 20 and 3 μm for the Zr–0.5%Cu–0.5%Cu alloy.

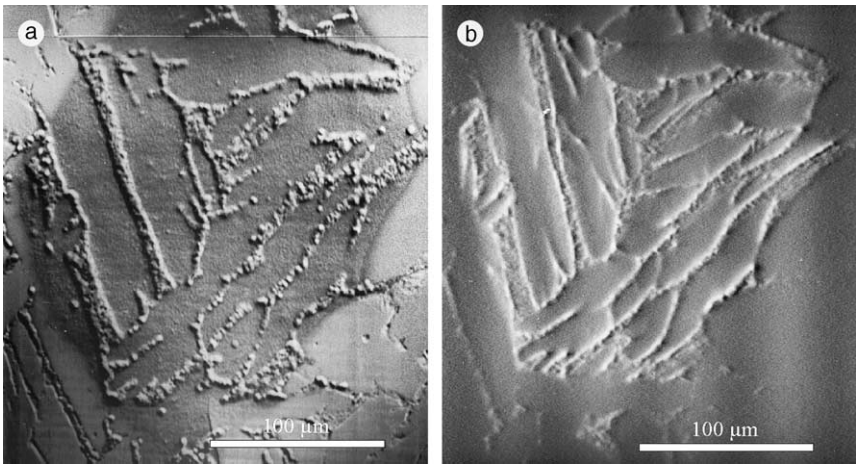

Fig. 1. SE and CL images of a Zr–0.1%Fe sample with metal substrate removed (a) SE on the metal side, (b) CL image corresponding to the image in part (a).

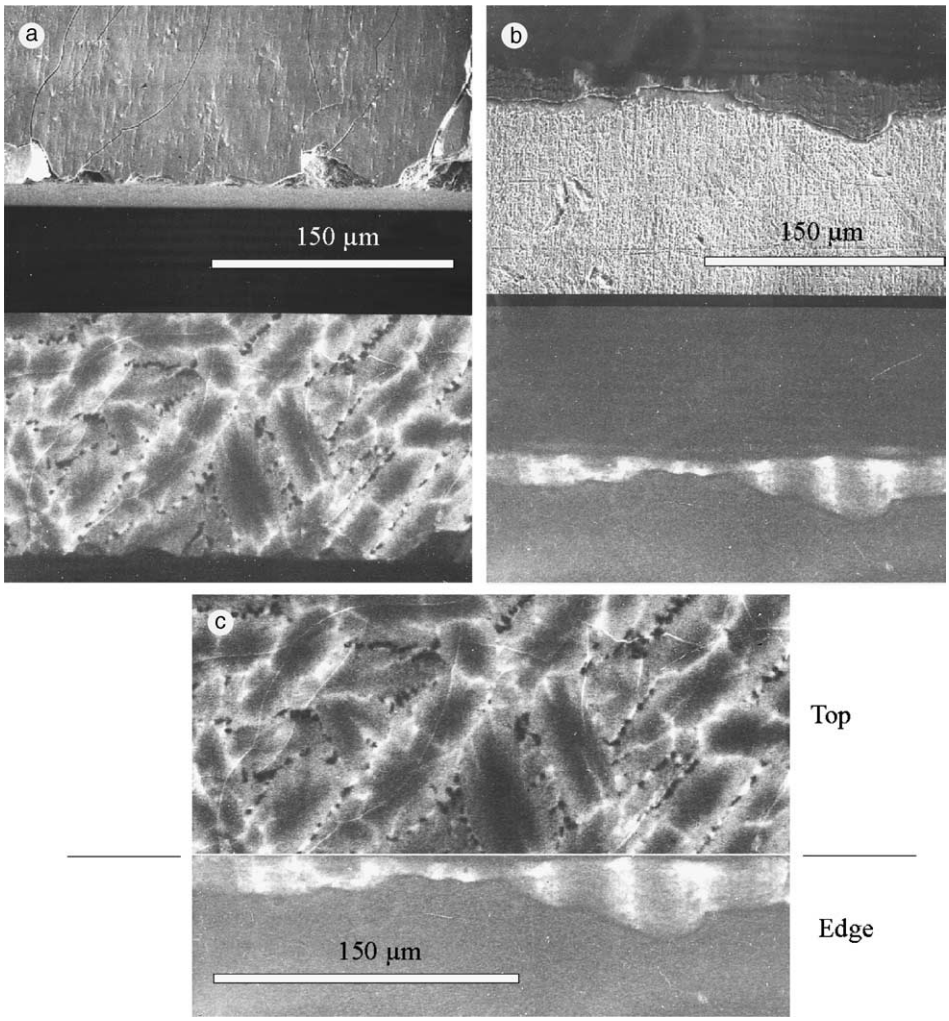

Fig. 2. SE and CL image of sample E, Zr–0.1%Fe, (a) SE and CL top view, (b) SE and CL edge view, (c) top and edge CL views matched together.

3.3. Involvement of Fe in luminescence emission

The origin of the luminescence emission has been discussed in an earlier publication [2]; essentially the results obtained from this study support the theory that alloying elements in conjunction with oxygen vacancies (T-defects) are responsible for the observed luminescence. There is strong evidence that Fe is involved in the luminescence process. This is most clearly shown when the CL images of the binary alloys with different dopants are placed side by side. The effect of alloying elements on the CL emission is seen in Fig. 3. Of the three major dopants (Fe, Cr, Ni), only the sample doped with Fe showed strong CL variations (Fig. 3(b)). The strong CL signals originated from grain boundaries and were especially strong near Zr–Fe intermetallic precipitates (black spots in the image). Micro-X-Ray analysis of these precipitates, results tabulated in Table 3, indicated a strong correlation between the Fe/Zr ratio and the luminescence intensity in the vicinity of the precipitates. To illustrate the relationship, the secondary electron and the corresponding CL image of the precipitates listed in Table 3 are shown in Fig. 4(a) and (b), respectively. It should be noted that the precipitates near high CL intensity areas are larger and thus may bias the Fe/Zr ratio because of electron penetration depth. This type of behaviour links Fe to the CL process, and is especially clear when looking at the CL images in Fig. 3. As further confirmation, earlier study of binary zirconium oxide powder doped with Fe was found to be luminescent [2]. Additional support for the involvement of Fe in the luminescence process with respect to the T-defect comes from data reported in literature. The T-defect, having an intrinsic emission

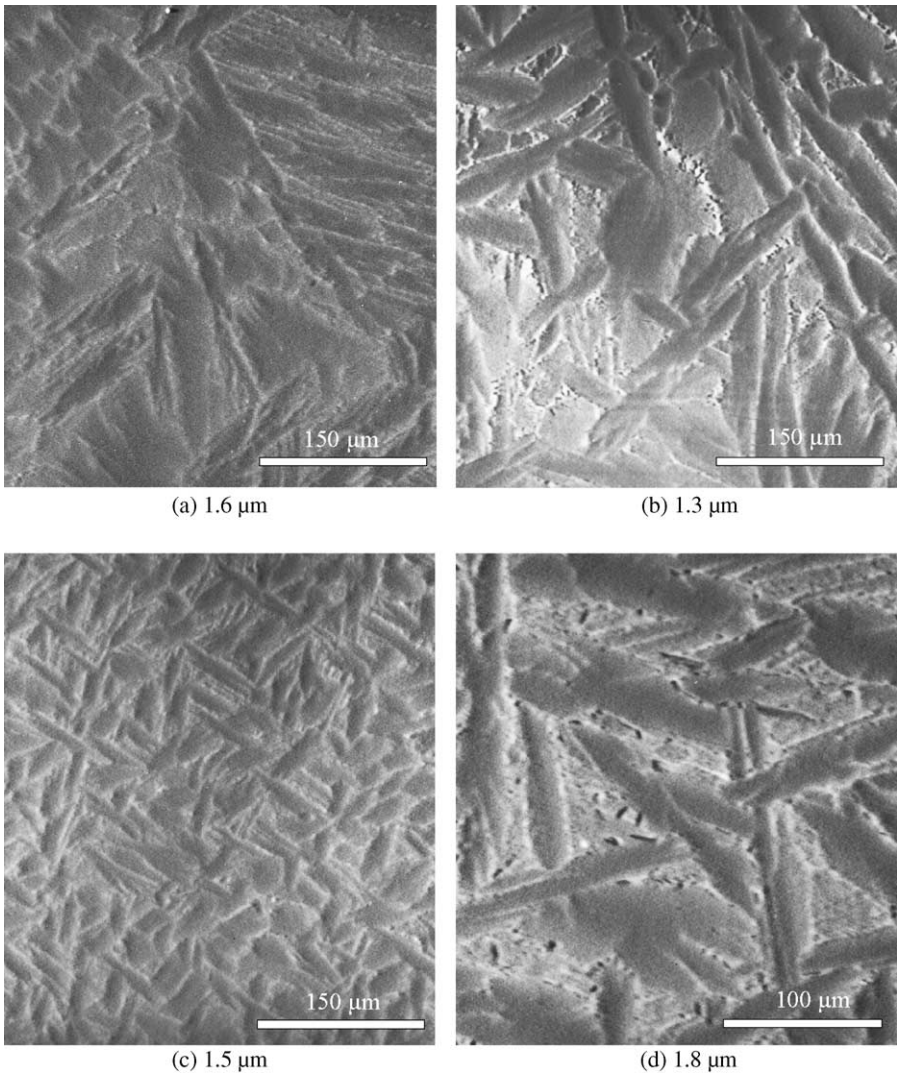

(a) 1.6 μm (b) 1.3 μm

(c) 1.5 μm (d) 1.8 μm

Fig. 3. CL images of (a) melted pure Zr, (b) Zr–0.1%Fe, (c) Zr–0.1%Cr, and (d) Zr–0.5%Ni (oxide thickness formed in 723 K air is shown below each image).

Table 3
List of the Fe(Kα)/Zr(Lα) peak ratios of precipitates shown in Fig. 4

Particle #	Fe/Zr ratio	CL intensity	Particle #	Fe/Zr ratio	CL intensity
1	0.73	Medium	6	0.35	Low
2	0.82	High	7	0.40	Low
3	1.02	High	8	0.41	Medium
4	0.86	Low	9	0.49	Medium
5	0.38	Low			

energy of ~2.2 eV, is commonly described in literature as a Zr^{3+} ion with two nearest neighbour oxygen vacancies in the opposite cube corners [11]. The true nature of the T-defect is still unclear and the subject of controversy, as investigators have correlated electron paramagnetic resonance (EPR) signals of the defect with different ion species in stabilised zirconia [12–14]. In the case of the Fe involvement in the luminescence process,

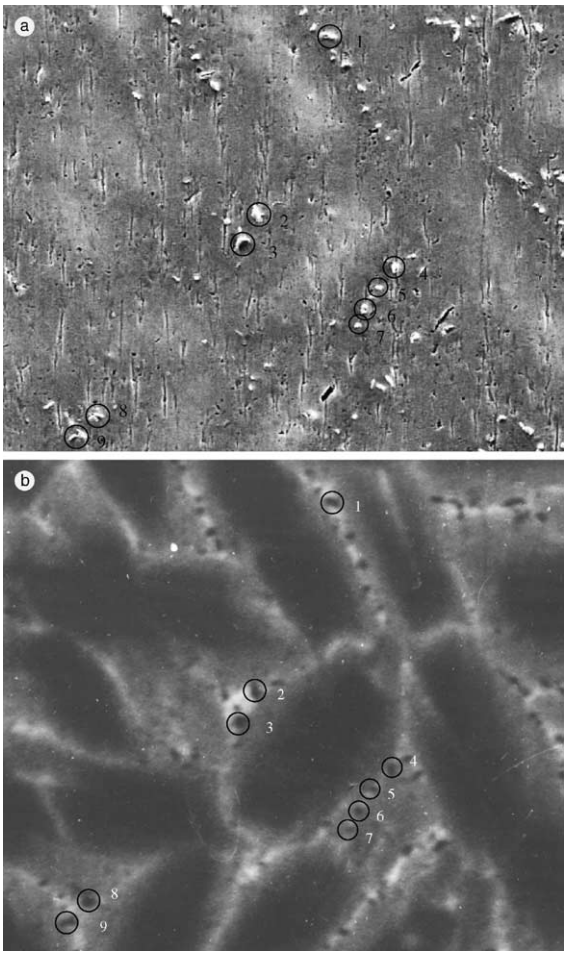

Fig. 4. Secondary electron (a) and the corresponding (b) CL image showing Zr–Fe precipitates.

investigation by other researchers of Fe stabilised zirconia, using iron-57 Mossbauer spectroscopy, showed the iron to be trivalent. These independent researchers have also proposed the theory of the substitution of Zr^{4+} by Fe^{3+} ions, in which oxygen vacancies would be needed to maintain charge neutrality [15]. The structure proposed by these researchers essentially describes the T-defect. In a separate EPR study, chromium was also found to enter the stabilised zirconia lattice as Cr^{3+} ion in a cation position in a six-fold nearest neighbour oxygen coordination [6,13]. As the T-defect is believed to be the source of intrinsic luminescence (electrons trapped at the T-defects may recombine with holes in the valance band), establishing the basis for a link between the two species (Fe and Cr) and the T-defect is important in explaining the cathodoluminescence observations. The idea that Fe is involved in the luminescence process is further supported by the report that Fe and Cr are attracted to oxygen vacancies [16,17], a perfect combination for the formation of T-defects. Since the T-defects have been correlated with multiple ion species, the creation of the defect by both iron and chromium is plausible. The luminescence observations reported in the earlier study conducted by the authors showed slight shifts in emission peak locations with different doping species. This suggests the existence of variations of the T-defects due to the substitution of the zirconium ion by different cation species. The concentrations of Fe and Cr involved in these phenomena must be quite small as no diffusion profiles for Fe around precipitates were detected by SIMS or AES mapping. However, both instruments have poor resolution on the scale observed here.

3.4. Distribution of Fe

With the above evidence, the involvement of Fe in the luminescence process can be explored further by studying its distribution in the oxide. Bright CL emissions originate only from the areas around the Zr_3Fe precipitates (which remain dark) and these emissions do not seem to change as the oxide thickens over time at 723 K. The absence of high CL emission areas in the pure Zr, ZrCr and ZrNi alloys indicates the low diffusion rate of Fe in the 723 K temperature range since the base Zr material contains 0.05% Fe. A published value of 190 nm for the diffusion distance of Fe was reported for an oxidation period of 41 days at 673 K [18]. Samples oxidised at 873 K all show high CL signals at the grain boundaries, indicating the diffusion of Fe to these locations (whether deliberately added or present as an impurity, Fig. 5). The segregation of Fe to the grain boundaries seems to be a continuous process as the oxide grows in the 873 K temperature range. In the early stages of oxidation at 873 K, the CL emission centres are not as well defined, and appear almost to be many tiny sites spread across the sample. As the oxide grows, the centres coalesce to form a more uniform luminescence image. This is most clearly shown in the lower two images in Fig. 6. The top two images of Fig. 6 show oxidation of the same sample (Zr–0.1%Fe) oxidised at 723 K to two different oxide thicknesses. Looking at these images, it is clear that there was very little change with increasing time in the CL features in the images of the oxides oxidised at 723 K, but a big change in the CL features in the oxides oxidised at 873 K as they thickened. This confirms the hypothesis of a low diffusivity of Fe at 723 K and a much higher diffusivity of Fe at 873 K in ZrO_2.

Samples of the as-received and as-received-β-annealed zirconium were also oxidised at 723 and 823 K. For the as-received sample, no localised CL signals were observed at grain boundaries, but were strong near cracks in the oxide, see Fig. 7(a)–(d). The sample oxidised at 873 K has a higher CL intensity at the cracks.

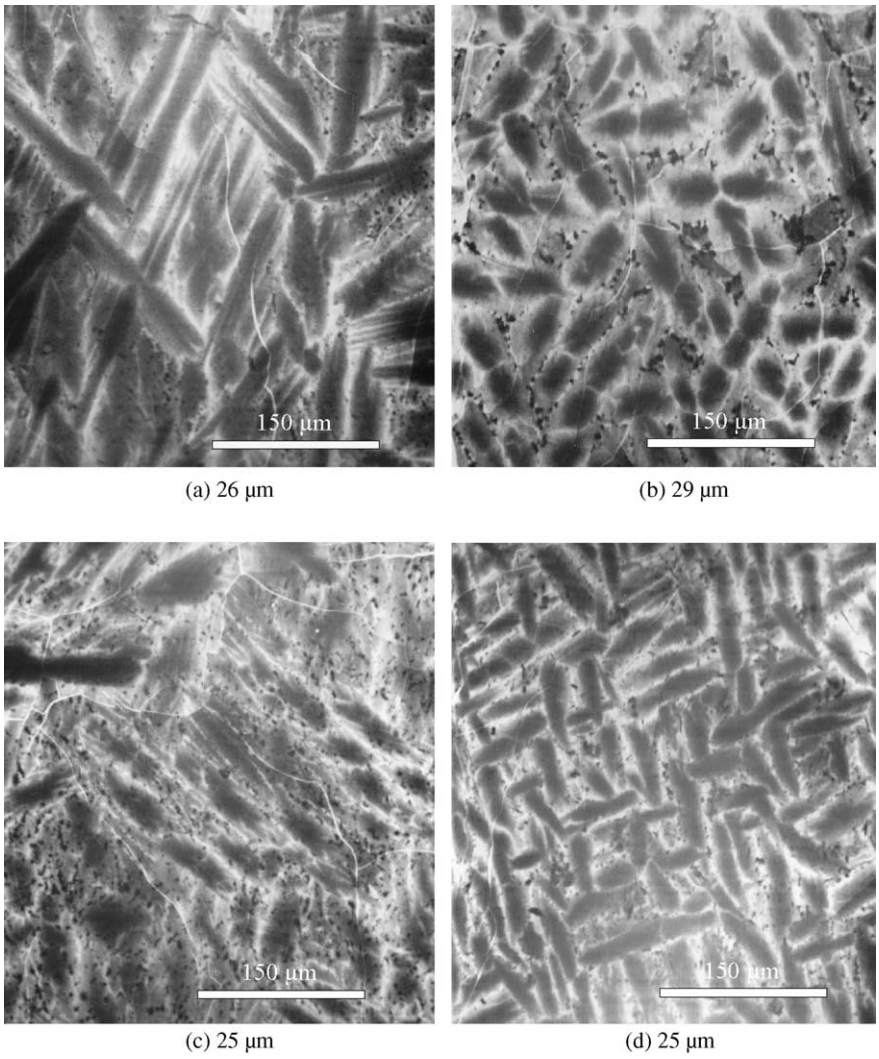

Fig. 5. CL images of samples oxidised in 873 K air, (a) melted as received pure Zr, (b) Zr–0.1%Fe, (c) Zr–0.1%Cr, and (d) Zr–0.1%Ni (oxide thickness is shown below each image).

For the as-received-β-annealed sample oxidised at 873 K, very strong CL signals originated from the grain boundaries and cracks (Fig. 7(e) and (f)). It is therefore reasonable to assume that the impurities present in the original material are responsible for this difference. Since Fe is the major impurity present in the 'pure Zr' material, and because of the linking of Fe to high CL intensity areas in oxidised ZrFe alloy specimens, it is reasonable to assume that Fe was involved in the luminescence process here. An additional point that should be made based on these images is the difference in the CL intensity at the cracks between samples oxidised at 723 and 873 K. It is only for the sample oxidised at 873 K that a high CL intensity at cracks is clearly seen. This once again supports the hypothesis of a longer diffusion distance through the oxide for Fe at 873 K than at 723 K. The documented diffusion of Fe toward a free surface supports the hypothesis that Fe is involved in the luminescence process [19,20]. However, it cannot be Fe present as Fe_2O_3 because powders doped with this and calcined at 1000 °C did not luminescence strongly. Heat treating at this temperature is known to produce a monoclinic polymorth structure with Fe segregation in the form of α-Fe_2O_3 [15]. The Fe, therefore, must be in some other chemical form, mostly likely as Fe doped ZrO_2 since the CL peaks are characteristic of ZrO_2 and probably in the form of an Fe/vacancy complex since the emissions are characteristic of a T-centre [6,11]. Unfortunately the quantities were too small to be resolved by SIMS or AES.

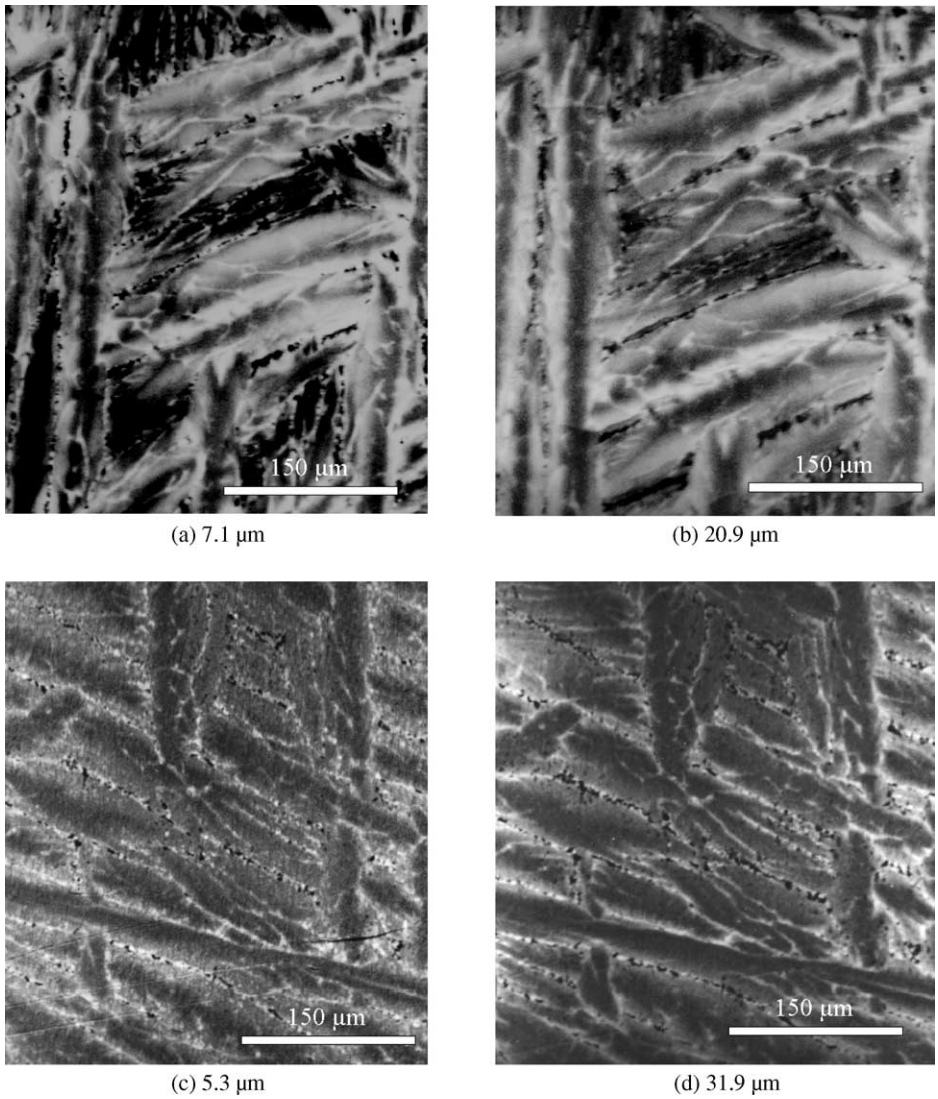

(a) 7.1 μm (b) 20.9 μm

(c) 5.3 μm (d) 31.9 μm

Fig. 6. Shows a comparison of CL images of a Zr–0.1%Fe sample, top images are oxidised at 723 K and bottom images are for oxidation at 873 K. Each pair of image is of the same area of the specimen (oxide thickness is shown below each image).

3.5. Effect of Sn

Although Sn is one of the main alloying elements in the Zircaloys, it was excluded from the initial investigation because it is completely soluble in the matrix at the concentrations present. A Zr–0.1%Sn sample (β-annealed) and a batch of Zircaloy-2 sample (containing ~1.5% Sn, in the as-received condition) were oxidised at 873 K. Images for the first of these samples are presented in Fig. 8. There are many cracks in the oxide in these images, and yet no high intensity CL was observed from these sites. Even though the Zr–0.1%Sn sample was β-annealed, there does not seem to be a very strong segregation of impurities to the grain boundaries as was seen in some of the other samples. The absence of high intensity CL emissions at the cracks would suggest either that Sn may be slowing down the diffusion of other impurity species such as Fe to the free surface or it is quenching the luminescence. However, there is no data available in literature that links the dependence of Fe diffusion in Zr to Sn. The even distribution of the CL emission in part (b) of the figure also supports the idea of a low diffusion rate in this sample.

3.6. Cyclic behaviour

Oxidation curves at 723 K for the different alloy samples and the corresponding CL intensity versus

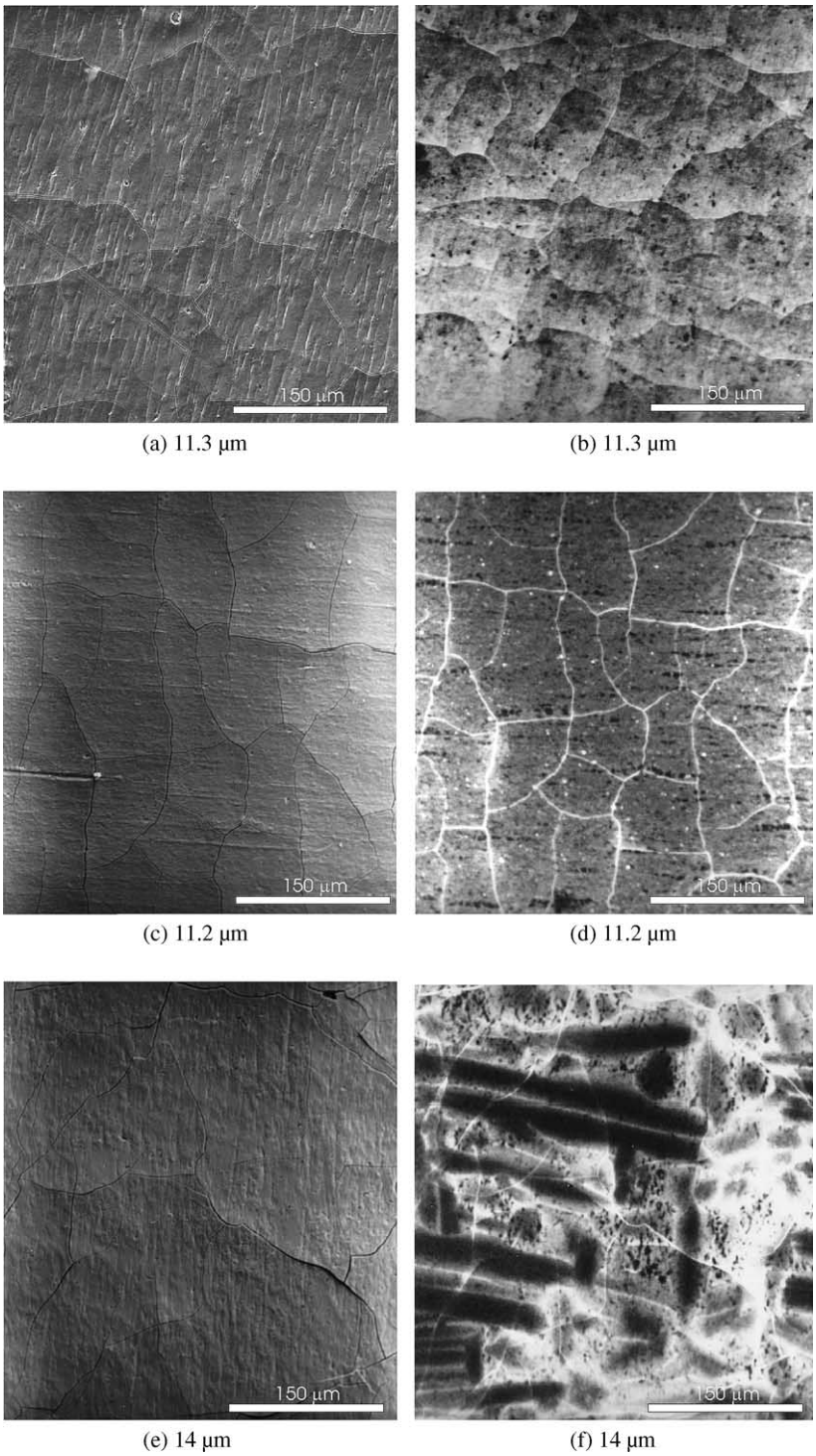

Fig. 7. SE and CL images of as received pure Zr samples oxidised at 723 K ((a) and (b)), 873 K ((c) and (d)), and images of a β-annealed pure Zr sample, oxidised at 873 K ((e) and (f)).

oxide thickness are plotted in Fig. 9. Cyclic behaviour reported in the literature is barely visible in the oxidation curves and only slightly pronounced in the CL intensity versus oxide thickness plots. This type of

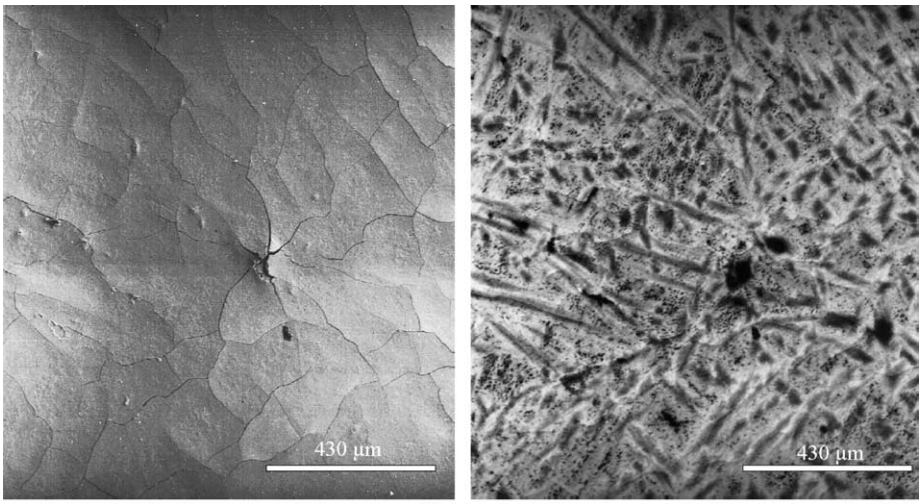

Fig. 8. Shows Se and CL images of a Zr–0.1%Sn alloy, oxidised at 873 K (17 μm oxide thickness).

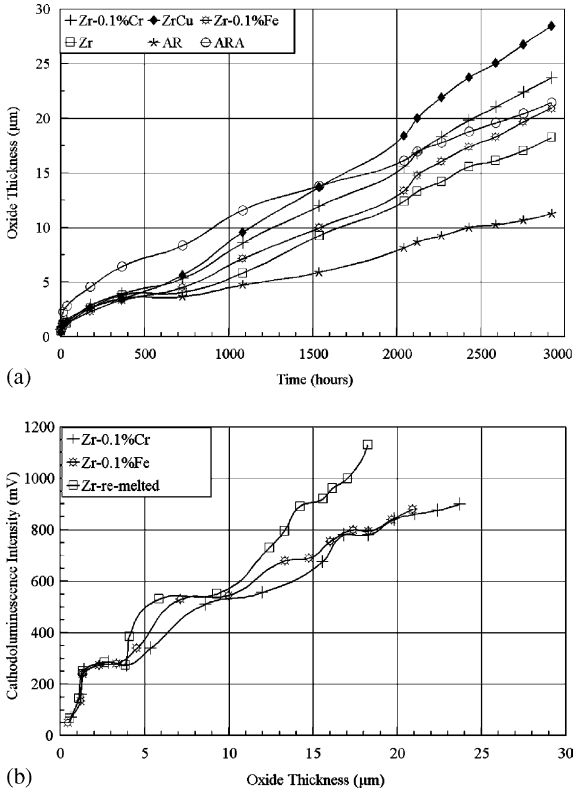

Fig. 9. Part (a) shows the oxidation curves at 723 K, part (b) shows the CL intensity plots versus oxide thickness.

behaviour is further diminished at 873 K oxidation temperature. The origin of this phenomenon is not well established in the literature. The cause of the cyclic behaviour has been extensively debated. The arguments are whether the cyclic behaviour is caused by cracks normal to the oxide surface that can pass most of the way through the oxide; by fine pores that form a network within the oxide [21,22], or by cracks that form parallel to the plane of the surface [23,24]. The cyclic behaviour has been observed by Godleswski [25], who measured the amount of tetragonal zirconia in the primarily monoclinic oxide as a function of the weight gain using X-ray diffraction and Raman spectroscopy. The cyclic behaviour could have implications for the origin of the CL emission and would raise the question as to whether one crystallographic form of the oxide is more luminescent than the other. Areas around a precipitate are thought to be stabilised as the tetragonal form by the presence of Fe. The presence of bright areas in the CL image near Fe precipitates might indicate that the tetragonal phase is more luminescent than the monoclinic. This might be related to the closer approach to an isotropic co-ordination of the zirconium ions by oxygen in the tetragonal compared with the monoclinic form of the oxide, especially if the c/a ratio is close to 1.0. The T-defect that appears to be the source of the luminescence has been characterised previously only in the case of the stabilised cubic form of ZrO_2, where the co-ordination polyhedron would be isotropic.

The cyclic behaviour is barely visible in the oxidation curves in this study due to the higher oxidation temperatures, but it is more visible in the CL emission intensity measurements for the 723 K oxidation and to a lesser extent for the samples oxidised at 873 K. The difficulty in observing the cyclic behaviour in the CL mode at the higher oxidation temperature is consistent with the observations from conventional weight gain

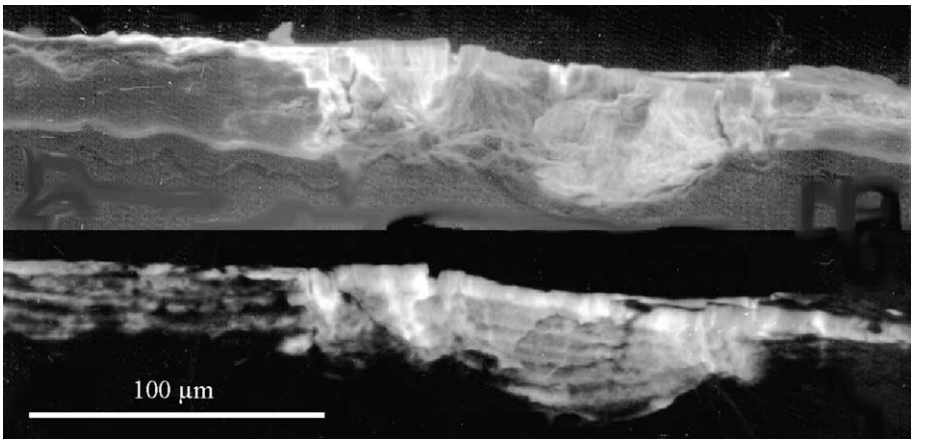

Fig. 10. SE and CL edge view of sample E, Zr–0.1%Fe oxidised in air at 873 K to an average thickness of 29 μm.

measurements. The reason for this difficulty may be due to the large number of pores nucleated (and pore network formation), which are not forming in synchronisation. Since a high CL intensity is often associated with coarse cracks in the oxide, the CL measurements are a more sensitive technique for detecting coarse cracking in the oxide than is the visibility of cycles in the weight gain curves. Secondary electron and CL cross-section images obtained in this study show that the cyclic behaviour is due to the formation of successive layers of coarse cracks both parallel to and perpendicular to the oxide surface. An example of such an image is shown in Fig. 10. To remove the doubt that the cyclic behaviour might be caused by the discontinuous weighing technique [1], a set of zirconium specimens were oxidised continuously in the furnace to the desired thickness, the cyclic behaviour is still clearly visible in these samples, thus can not have been caused by the discontinuous weighing technique.

4. Conclusions

The ability of the CL technique to show detailed structural/chemical information for the zirconium oxide system shows the technique could be a useful tool in studying some low alloying element concentration distributions. The results presented here clearly show strong CL contrast, which arises primarily from signals at the grain boundaries, areas adjacent to Fe-containing precipitates, and at cracks, where there is known segregation of alloying elements. This supports the hypothesis that alloying elements in conjunction with oxygen vacancies are involved in the luminescence process in the zirconium oxide system. The redistribution of alloying elements, particularly iron, has been clearly shown in CL images of samples oxidised at 873 K. Cyclic behaviour observed in the oxidation kinetic curves of only low temperatures is found in the CL emission intensity curves at all temperatures and appears to be caused by successive lateral cracking to form layers in the oxide.

References

[1] Waterside corrosion of zirconium alloys in nuclear power plants, IAEA-TECDOC-996, IAEA, Vienna, 1998.
[2] H.K. Yueh, B. Cox, Luminescence properties of zirconium oxide films, J. Nucl. Mater. 323 (2003) 57.
[3] C. Bonola, P. Camagni, N. Omenetto, G. Samoggia, J. Luminescence 48&49 (1991) 797.
[4] K.M. Ganguly, S. Sarkar, S.N. Bhattacharyya, J. Chem. Soc., Chem. Commun. (1993) 682.
[5] G.M. Phatak, K. Gangadharan, H. Pal, J.P. Mittal, Bull. Mater. Sci. 17 (1994) 163.
[6] P.J. Alonso, R. Alcala, J. Casas-Gonzalez, R. Cases, V.M. Orera, J. Phys. Chem. Sol. 50 (1989) 1185.
[7] J.F. Sarver, J. Electrochem. Soc. 113 (1966) 124.
[8] S.E. Paje, M.A. Garcia, J. Llopis, M.J. Saavedra, C. Parada, Phys. Stat. Sol. (a) 148 (1995) K45.
[9] S.E. Paje, J. Llopis, Appl. Phys. A 57 (1993) 225.
[10] S.E. Paje, J. Llopis, Appl. Phys. A 59 (1994) 569.
[11] R.I. Merino, V.M. Orera, Solid State Ionics 76 (1995) 97.
[12] J. Shinar, D.S. Tannhauser, B.L. Silver, Solid State Commun. 56 (2) (1985) 221.
[13] V.M. Orera, R.I. Merino, Y. Chen, R. Cases, P.J. Alonso, Phys. Rev. B 42 (1990) 9782.
[14] R.I. Merino, V.M. Orera, E.E. Lomonova, S.Kh. Batygov, Phys. Rev. B 52 (1995) 6150.
[15] F.J. Bery, M.H. Loretto, M.R. Smith, J. Solid State Chem. 83 (1989) 91.
[16] P. Li, I.W. Chen, J. Am. Ceram. Soc. 77 (1994) 118.
[17] A. Hanazaki, T. Takayama, H. Anada, S. Hinotani, J. Jpn. Inst. Met. 60 (1996) 113.
[18] X. Iltis, F. Lefebvre, C. Lemaignan, J. Nucl. Mater. 224 (1995) 121.

[19] F.J. Berry, J.H. Loretto, M.R. Smith, J. Sol. Stat. Chem. 83 (1989) 91.
[20] R.V. Wilhem Jr., D.S. Howarth, Am. Ceram. Soc. Bull. 58 (1979) 228.
[21] B. Cox, in: M.G. Fontana, R.W. Staehle, (Eds.), Adv. in Corr. Sci. and Tech., vol. 5, Plenum, NY, 1976, p. 173.
[22] B. Cox, J. Nucl. Mater. 29 (1969) 50.
[23] S.W.S. McKeever, Thermoluminescence of Solids, Cambridge University, Cambridge, 1985.
[24] B. Cox, J. Nucl. Mater. 41 (1971) 96.
[25] J. Godlewski, in: A.M. Garde, E.R. Bradley (Eds.), Zirconium in the Nuclear Industry: Tenth International Symposium, ASTM STP 1245, American Society for Testing and Materials, Philadelphia, 1994, p. 663.